HHS Public Access

Author manuscript

Biomaterials. Author manuscript; available in PMC 2018 April 01.

Published in final edited form as:

Biomaterials. 2017 April ; 123: 142–154. doi:10.1016/j.biomaterials.2017.01.037.

Perivascular Extracellular Matrix Hydrogels Mimic Native Matrix Microarchitecture and Promote Angiogenesis via Basic Fibroblast Growth Factor

George R. Fercana[#], **Saigopalakrishna Yerneni**[#], **Marie Billaud**, **Jennifer C. Hill**, **Paul VanRyzin**, **Tara D. Richards**, **Brian M. Sicari**, **Scott A. Johnson**, **Stephen F. Badylak**, **Phil G. Campbell**, **Thomas G. Gleason**, and **Julie A. Phillippi**

Department of Cardiothoracic Surgery, McGowan Institute for Regenerative Medicine, University of Pittsburgh School of Medicine, Pittsburgh, PA

Department of Bioengineering, Center for Vascular Remodeling and Regeneration, University of Pittsburgh School of Medicine, Pittsburgh, PA

Department of Biomedical Engineering, Carnegie Mellon University, Pittsburgh, PA

[#] These authors contributed equally to this work.

Abstract

Extracellular matrix (ECM)-derived bioscaffolds have been shown to elicit tissue repair through retention of bioactive signals. Given that the adventitia of large blood vessels is a richly vascularized microenvironment, we hypothesized that perivascular ECM contains bioactive signals that influence cells of blood vessel lineages. ECM bioscaffolds were derived from decellularized human and porcine aortic adventitia (hAdv and pAdv, respectively) and then shown have minimal DNA content and retain elastin and collagen proteins. Hydrogel formulations of hAdv and pAdv ECM bioscaffolds exhibited gelation kinetics similar to ECM hydrogels derived from porcine small intestinal submucosa (pSIS). hAdv and pAdv ECM hydrogels displayed thinner, less undulated, and fibrous microarchitecture reminiscent of native adventitia, with slight differences in ultrastructure visible in comparison to pSIS ECM hydrogels. Pepsin-digested pAdv and pSIS ECM bioscaffolds increased proliferation of human adventitia-derived endothelial cells and this effect was mediated in part by basic fibroblast growth factor (FGF2). Human endothelial cells cultured on Matrigel substrates formed more numerous and longer tube-like structures when supplemented with pAdv ECM bioscaffolds, and FGF2 mediated this matrix signaling. ECM bioscaffolds derived from pAdv promoted FGF2-dependent *in vivo* angiogenesis in the chick chorioallantoic membrane model. Using an angiogenesis-focused protein array, we detected 55 angiogenesis-related proteins, including FGF2 in hAdv, pAdv and pSIS ECMs. Interestingly, 19 of these factors were less abundant in ECMs bioscaffolds derived from aneurysmal specimens of human aorta when compared with nonaneurysmal (normal) specimens. This study reveals that Adv

Corresponding author: Julie A. Phillippi, PhD 450 Technology Drive, Suite 300 Pittsburgh, PA 15219, Phone: 412-624-6704, Fax: 412-624-5363.

ECM hydrogels recapitulate matrix fiber microarchitecture of native adventitia, and retain angiogenesis-related actors and bioactive properties such as FGF2 signaling capable of influencing processes important for angiogenesis. This work supports the use of Adv ECM bioscaffolds for both discovery biology and potential translation towards microvascular regeneration in clinical applications.

Keywords

adventitia; extracellular matrix; hydrogel; endothelial cell; tube formation; angiogenesis; aneurysm

Introduction

Extracellular matrix (ECM) bioscaffolds are tissue-specific biomaterials with inherent bioactivity and native structural features. These properties enable their desirable use as three-dimensional *in vitro* cell culture substrates for biologic discovery of cellular mechanisms or as disease models. Importantly, these decellularized tissues show promise for therapeutic tissue regeneration in a variety of applications. [1-7] Development of decellularized native tissues led to the production of tissue-engineered scaffolds which retained basement membrane proteins such as collagen type IV, laminin, and fibronectin that enhance cellular adhesion [8, 9] and invoke signaling to influence cellular differentiation and regenerative potential [10-12]. Growth factors including transforming growth factor-beta, basic fibroblast growth factor (FGF), hepatocyte growth factor and vascular endothelial growth factor (VEGF) persist in their bioactive form within ECM bioscaffolds after sterilization. [13-17] Additionally, degradation of ECM bioscaffolds releases matricryptic peptides that invoke biologic activity. [18] ECM bioscaffolds guide stem cell differentiation through growth factor retention and unique matrix compliance, [19-23] which together comprise tissue-specific microenvironments that are advantageous for regeneration. [24]

The potential for ECM bioscaffolds to invoke angiogenesis is of particular importance for regenerative medicine applications. [13, 25] Although the vasculogenic and angiogenic mechanisms of ECM bioscaffolds are not fully understood, gradual release of growth factors during ECM degradation is a likely mechanism of action. [13] Since immobilized growth factors secreted by the resident cells fortify ECM, [26, 27] vascular ECM is a viable candidate biomaterial for invoking vasculogenesis and angiogenesis. The adventitia of blood vessels is a perivascular microenvironment that is heterogeneous in both form and function. Not only does the adventitia provide the majority of biomechanical strength to the vessel by nature of the woven network of fibrous proteins of the ECM, but it also serves as a progenitor cell niche. [28, 29] Furthermore, the diversity of cell composition in the vascular adventitia renders this ECM microenvironment a prime candidate for a multitude of desirable bioactive effects on blood vessel cell populations. [28, 30] Understanding the role of the adventitial ECM in vascular physiology will provide insight into cardiovascular disease particularly by exploring ECM bioscaffolds derived from human adventitia. Porcine adventitial ECM (pAdv) bioscaffolds, with their greater availability, can be utilized to harness their intrinsic bioactivity to develop potentially regenerative therapeutics.

This study tested the hypothesis that perivascular ECM contains bioactive signals that influence cells of blood vessel lineages. We characterized the composition and gelation kinetics of ECM hydrogel biomaterials formulated from human and porcine decellularized aortic adventitia and evaluated the signaling activity of porcine ECM bioscaffolds in processes related to angiogenesis using primary adventitia-derived human endothelial cell culture models, tube-forming *in vitro* assays, and an *in vivo* angiogenesis model. Porcine small intestinal submucosa (pSIS) was chosen as a control ECM due to its prior thorough characterization and current utilization as a clinically-relevant bioscaffold [31-34]. Our findings reveal several biomimetic features of perivascular ECM that may render these natural biomaterials useful for discovery biology and regenerative medicine applications.

Materials and Methods

2.1 Tissue Collection

Human ascending thoracic aorta specimens (n=40 patients) were collected during ascending aortic replacement operations or heart transplants with informed patient consent and approval of the institutional review board or from organ donors via the Center for Organ Recovery and Education. Acquisition of all human specimens was in accordance with the Helsinki Declaration of 1975, as revised in 1983. Following excision, tissue specimens were placed in saline on ice and transported to the laboratory. Specimens were collected from 22 males and 18 females ranging in age from 17 to 82 years. Porcine ascending aortic specimens were obtained from a commercial source (Tissue Source, Lafayette, IN) and shipped on wet ice. Porcine SIS specimens were obtained from a local abattoir (Thoma Meat Market, Saxonburg, PA) and prepared as previously described. [35, 36] Upon acquisition in the laboratory, all specimens were promptly stored at −80°C until use.

2.2 Decellularization of Aortic Adventitia

Adventitial ECM bioscaffolds were prepared from decellularized aortic tissue specimens from 39 patients and two pigs. The adventitial layer was delaminated from the media and decellularized using a previously established method. [37] Briefly, the adventitial specimens were incubated in a solution of 8mM CHAPS (3-[(3-cholamidopropyl) dimethylammonio]-1-propanesulfonate, Thermo Fisher Scientific, Waltham, MA), 1M NaCl (Thermo Fisher Scientific), and 25mM EDTA (ethylenediaminetetracetic acid, Thermo Fisher Scientific) for 24 hr at 37°C, followed by washing in 1x PBS (phosphate buffered saline, Thermo Fisher Scientific) then in deionized water (dH_2O). The tissue was then placed on a shaker for 1 hour in a solution containing 0.1% trypsin (Amresco, LLC, Solon, OH) and 0.04% EDTA, rinsed in dH_2O, then shaken in a solution of 0.5% SDS (sodium dodecyl sulfate, Thermo Fisher Scientific), 1M NaCl, and 25mM EDTA for 24 hr, followed by washing in 1x PBS and dH_2O. The tissue was then placed on a shaker in a solution of 0.1% peracetic acid (Rochester Midland Corporation, Rochester, NY) and 4% ethanol, followed by rinsing with 1x PBS and dH_2O before freezing overnight at −80°C and lyophilizing. Decellularized aortic adventitia from human and porcine aorta (here on referred to as hAdv and pAdv ECM bioscaffolds) was lyophilized and finely ground to produce an ECM bioscaffold powder for further enzymatic digestion. SIS ECM bioscaffold was

prepared previously as described elsewhere. [35, 36] Powdering and gelation of SIS utilized the same procedures described in this report.

2.3 Qualitative and Quantitative Assessment of DNA Content

Remnant DNA content was quantified from 25 mg of powdered Adv ECM bioscaffolds from porcine (2 pigs, pooled) and human aorta (4 patient specimens, pooled) using the QIAamp DNA Mini Kit (QIAgen, Germantown, MD) according to the manufacturer's instructions. Final elution volume was 50 μL Buffer AE. Qubit 2.0 (Thermo Fisher Scientific) was utilized to quantify the concentration of dsDNA in each extract. DNA extracts from 1.2 mg dry tissue weight of powdered ECM bioscaffolds and extracts from 1.2 mg wet tissue weight from native aorta were electrophoresed on a 1% agarose (Thermo Fisher Scientific) gel containing 0.003% (v/v) ethidium bromide (Sigma Life Science, St. Louis, MO) and visualized under UV light on a Chemidoc XRS Bioimaging Station (Bio-Rad, Hercules, CA)

2.4 Digestion of Powdered ECM Bioscaffolds

Adv and pSIS ECM bioscaffold powders were digested at a concentration of 20 mg/mL by stirring at 1600 RPM at room temperature for 24 hr in a 0.01 N hydrochloric acid solution (pH 2, Thermo Fisher Scientific) containing 1 mg/mL pepsin from porcine gastric mucosa (~2000-2300 U/mg, Sigma). After 24 hr, the ECM digests were either immediately used for gelation kinetics assays or stored at −20°C for future use.

2.5 Detection of Collagen and Elastin Content

Pepsin-soluble collagen was extracted from native adventitia and from adventitia-derived ECM bioscaffold powder using 0.1mg/mL pepsin in 0.5M acetic acid overnight at 4°C. After isolation and concentration steps, the amount of pepsin-soluble collagen was determined in each sample as previously described [38] using the Sircol Soluble Collagen assay (Biocolor Ltd, UK), according to the manufacturer's instructions. The amount of pepsin-soluble collagen determined in each extract was normalized to weight of wet tissue or weight of Adv ECM bioscaffold powder.

The amount of α-elastin was determined as described before [38] using the Fastin Elastin assay (Biocolor), according to the manufacturer's protocol. Insoluble elastin was converted to water soluble α-elastin by subjecting native adventitia and Adv ECM bioscaffold powder to three successive elastin extractions of one hour each, in 0.25M oxalic acid at 100°C. The amount of α-elastin determined in each extract was normalized to weight of wet tissue or weight of Adv ECM powder.

2.6 Formation of ECM Bioscaffold Hydrogels

Hydrogels were formulated from ECM bioscaffold digests according to an established method [39] and with all preparations performed on ice. Briefly, the digest was diluted to the desired final concentration and neutralized to a pH of 7.4 ± 0.2 in a solution of 10x PBS and 0.1 N NaOH (sodium hydroxide, Thermo Fisher Scientific).

2.7 Hydrogel Gelation Kinetics

Turbidimetric hydrogel gelation kinetics were determined for porcine and human Adv ECM bioscaffold-derived hydrogels (4-16 mg/mL) as described previously. [39] Optical density readings from 100 μL aliquots of neutralized ECM digest were obtained in triplicate every 2 minutes at 405 nm for up to 2 hr using a spectrophotometer (TECAN, Germany). Normalized absorbance (NA) was determined by the following equation:

$$NA = \frac{A - A_0}{A_{max} - A_0}$$

where 'A' represents the absorbance reading at a particular time point, 'A_0' represents the initial absorbance and 'A_{max}' represents the maximum absorbance. Additional metrics of ECM gelation determined include: the time required for 50% gelation, defined as '$t_{1/2}$'; the lag phase 't_{lag}', determined via extrapolation of the linear portion of the normalized absorbance curve; and the gelation speed 'S', calculated as the maximum slope of the growth region for the normalized absorbance curve.

2.8 Morphological Ultrastructure Characterization of Hydrogels

hAdv, pAdv, and pSIS ECM bioscaffold hydrogels were prepared at 8mg/mL on 12 mm round cover glass (Thermo Fisher Scientific) and fixed in 2.5% glutaraldehyde (Electron Microscopy Sciences, Hatfield, PA) for 1 hour. Fixed hydrogels were rinsed three times for 15 minutes in 1x PBS, treated in osmium tetroxide for 1 hour, and further rinsed three times for 15 minutes in 1x PBS before dehydration in graded ethanol series for 15 minutes each (30%, 50%, 70%, 90%, 100%). Dehydrated specimens were then critical point dried with supercritical CO_2 (Leica Biosystems, Buffalo Grove, IL), allowing 15 minutes for processed hydrogels to soak before each purge cycle. Following critical point drying, samples were sputter coated with gold-palladium (Cressington Scientific Instruments, Watford, England) at a thickness of 4.6 nm. The surface morphology of hAdv, pAdv and pSIS ECM hydrogels was then examined using a JSM 6335F scanning electron microscope (Jeol USA, Inc., Peabody, MA) at 5,000x and 10,000x total magnification and compared with intact specimens of decellularized native human adventitia.

2.9 Isolation and Culture of Primary Adventitia-Derived Human Endothelial Cells

Primary endothelial cells were isolated from the adventitia of a human specimen of thoracic aorta from a healthy donor. Upon specimen acquisition in the lab within 1-2 hr of harvest, the adventitia was immediately stripped away from the medial layer and rinsed twice in ice-cold 1X PBS with 1% (v/v) penicillin/streptomycin and 1% (v/v) Fungizone (Invitrogen). Tissue was then finely minced using safety scalpels and rinsed in 1X PBS. The tissue and PBS were placed in a 70 μm molecular sieve. The pass-through was collected and held at 37°C while remaining tissue was digested in DMEM (Life Technologies) containing 0.4% (w/v) collagenase type IV (Worthington Biochemical Corporation, Lakewood, NJ) and 350 KU/mL DNase I (Sigma) for 30 min at 37°C with gentle agit ation. The digestion medium and tissue was passed through a 70 μm sieve and tissue was returned to fresh digestion medium for another 30 min at 37°C with gentle agitation. Following a fina l straining

through a 70 μm sieve and wash with 1X PBS, all filtrates were pooled and centrifuged at 400 g for 10 min at 4°C. Cells were plated in 75 cm^2 culture flasks in endothelial growth medium (EGM, Cell Applications, San Diego, CA). Gentamycin (250 μg/mL, Thermo Fisher Scientific) was added for 24-48 hr. Cells were maintained in a humidified incubation chamber at 37°C and 5% CO 2 and expanded for 1-2 passages. Primary endothelial cells were isolated from parent culture using fluorescence-activated cell sorting (FACS).

For FACS-based isolation of endothelial cells, expanded adventitial cells were pelleted (~1-4 × 10^6 cells), incubated in 1 μL neat mouse serum (Sigma) on ice, protected from light, and labeled with the following fluorochrome-conjugated monoclonal mouse anti-human antibodies (2 μL per antibody): CD31-PE-Cy7 (Biolegend, San Diego, CA, #303117), CD45-APC-Cy7 (BD Biosciences, San Jose, CA, #348805), and CD34-ECD (#BD2709U), and CD56-PE-Cy5 (IM2654, both from Beckman Coulter, Indianapolis, IN). DAPI (200 ng/mL) was added to unfixed and unpermeabilized cell suspensions just prior to sorting to discriminate live from dead/apoptotic cells. Cells were sorted using three of a five-laser MoFlo Astrios high speed cell sorter (Beckman Coulter, University of Pittsburgh Cancer Institute Flow Cytometry Core Facility) enclosed in a Class II biosafety cabinet. Cells were sorted as previously described [40] on the basis of a mature endothelial surface proteome of ($CD56^-$/$CD45^-$/$CD34^-$/$CD31^+$) into 6-well plates containing EGM with gentamicin, expanded for 1-2 passages with media replenishment every second day until cryopreservation.

2.10 Cell Proliferation Assay

Sorted primary human adventitia-derived endothelial cells (<P9) were seeded in 96 well plates at a density of 5 × 10^3 cells/well in EGM. Cells were cultured for 72 hr in the presence or absence of freshly-digested pAdv or pSIS ECM bioscaffolds (10 μg/mL). An inhibitor of FGF2 signaling, PD173074 (Sigma) was administered to cells in parallel cultures at a final concentration of 100 nM (prepared from a 10 mg/mL stock in dimethyl sulfoxide (DMSO)). Cells cultured in EGM alone and equivalent volumes of pepsin HCl digestion buffer (control for ECM treatments) and DMSO (vehicle control for FGF2 inhibitor treatments) were performed in parallel. Cell proliferation was assessed using a commercial MTS conversion assay (CellTiter 96® AQueous One Solution Cell Proliferation Assay, Promega, Madison, WI) performed according to the manufacturer's instructions.

2.11 Endothelial Cell Branching Assay

Cell culture substrates were prepared by coating the surface of wells in a 48-well culture plate with growth factor-reduced (GFR) Matrigel (Corning) prepared in the presence or absence of freshly-digested pAdv or pSIS ECM bioscaffold (250 μg/mL). Gelation was allowed to occur in a humidified 37°C incubator for 1 hr. Primary human adventitia-derived endothelial cells were seeded in triplicate on gel-based substrates at a density of 1.5 × 10^4 cells/cm^2 in EGM. Digestion buffer (1mg/ml pepsin in 0.1N HCL) and DMSO only controls were performed in adjacent wells. Where indicated, cells were treated with 100 nM PD173074. To assess endothelial cell branching formation of tube-like structures, large frame images were captured at 7 hr post-cell seeding using a Nikon Eclipse TE2000-E microscope equipped with an imaging array CoolSNAP ES2 monochrome camera and NIS

Elements Software (Nikon Inc., Melville, NY). Total number and length of tube-like structures were quantified using NIS Elements Software.

2.12 Chick Chorioallantoic Membrane (CAM) Model of In Vivo Angiogenesis

The CAM assay was modified from our established protocols. [41, 42] White Leghorn eggs were purchased from a local farm and incubated at 37°C and 70% humidity (G.Q.F. Manufacturing Co., Savannah, GA). On day 3 of incubation, eggs were cracked into sterile petri dishes and incubated for 10 days. Fibrin scaffolds to be placed on the chicken chorioallantoic membrane (CAM) were prepared similar to previously described methods. [43-45] Briefly, final concentrations of 5 mg/mL bovine fibrinogen, 1 U/mL aprotinin (both from Enzyme Research Labs, South Bend, IN) were buffered in 1X PBS, pH 7.4. Addition of digestion buffer (1mg/mL pepsin in 0.1N HCL) to fibrin scaffolds served as a negative control for angiogenic response. The final concentration of pAdv ECM bioscaffold in fibrin gels was varied from 50 μg/mL to 500 μg/mL in the presence or absence of the FGF2 inhibitor PD173074 (100 nM in DMSO) or vehicle control (0.05% (v/v) DMSO). Scaffold components were mixed and incubated at 37°C for 30 min. Human thrombin (Enzyme Research laboratory, South Bend, IN) was added to 1 U/mL to initiate fibrin polymerization and incubated at 37°C for 60 min in a 48-well plate (Corning, NY). Fibrin scaffolds supplemented with the test materials were placed on the CAM and incubated at 37°C with 70% humidity.

After 72 hr on the CAM, bright field images of the scaffolds and surrounding vasculature resulting from the angiogenic response were captured using a 3MP color camera mounted on a stereomicroscope (AmScope, Irvine, CA) at a 7.5X magnification. Endothelial cells of the chick vasculature were labelled by micro-injecting DyLight® 650-labeled tomato lectin (Vector labs, Burlingame, CA) and incubated for 15 min prior to excising the scaffold and the surrounding CAM. The harvested tissue was fixed in 10% neutral-buffered formalin (Sigma, St. Louis, MO) for 48 hr, washed in 1X PBS thrice and cryoprotected for 72 hr in 30% sucrose solution before processing for histological evaluation. The scaffolds were dissected in half, embedded in Tissue-Tek OCT (Sakura Finetek USA Inc., Torrance, CA) and 60 μm thick sections were cut using a Microm HM500OM cryostat microtome (Thermo Fisher Scientific). The sections were stained with Hoechst 33342 solution (Thermo Fisher Scientific) and imaged using Zeiss LSM 880 confocal microscope using a 10X objective. Tile scanning was performed and the images were stitched using ZEN black microscope and imaging software (Carl Zeiss Microscopy, Thornwood, NY).

2.13 Protein Array

Decellularized human adventitia from normal (n=7 patients) and aneurysmal (n=28 patients) aortic specimens, and porcine adventitia and SIS were analyzed for the presence of angiogenesis-related proteins using the Protein Profiler™ Array Human Angiogenesis Kit (R&D Systems, Minneapolis, MN) according to the manufacturer's instructions. Briefly, lyophilized ECMs were resuspended in RIPA buffer containing protease inhibitors and homogenized using a douncer. Total protein concentration was assessed using a bicinchoninic acid assay (Thermo Scientific) and 300 μg of total protein was used as input

for the array. Densitometry measurements were made from duplicate spots of each protein using ImageJ software (National Institutes of Health, USA).

2.14 Statistical Analysis

All experiments were repeated at least two times. Pairwise comparisons in quantitative measures were made between treatments and controls using an unpaired two-tailed Student's T test. Quantitative data provided in the results section represent the mean ± standard deviation. A p value of less than 0.05 was considered statistically significant.

Results

3.1 Adv Bioscaffold Characterization

Adventitia stripped from porcine and human aortic media were decellularized, lyophilized, and ground into a fine powder (Fig. 1A). pH-neutralized pepsin-digested ECM bioscaffolds formed hydrogels at 37°C (Fig. 1B). Qualitative assessment of DNA content using gel electrophoresis revealed lower DNA content in hAdv and pAdv bioscaffolds when compared with native specimens (Fig. 1C). Total DNA content was found to be <40 ng/mg tissue and <350 ng/mg dry tissue weight for hAdv and pAdv bioscaffolds, respectively and <80 ng/mg for pSIS bioscaffolds. These pAdv and hAdv bioscaffolds also retained appreciable collagen and α-elastin (Table 1).

3.2 Adv Bioscaffold Hydrogels Exhibit Fiber-like Microarchitecture Similar to Native Adventitia

The matrix ultrastructure of decellularized human adventitia was investigated before the grinding and lyophilization steps of the ECM bioscaffold preparation (Fig. 2A, B). Observation of these specimens via scanning electron micrographs revealed an acellular fibrous microarchitecture (Fig. 2A, B). A similar microarchitecture was also observed in hydrogels produced from digested hAdv (Fig. 2C, D) and pAdv (Fig. 2E, F) bioscaffolds, which exhibited a thinner and straighter morphology. In comparison, hydrogels produced from digested pSIS bioscaffolds displayed thicker, more undulated fibers, with additional globular ECM apparently adhered to the fibers (Fig. 2G, H). The native-like fibrous matrix microarchitecture of adventitia was recapitulated following the decellularization, lyophilization, grinding, digesting, and gelation processes utilized to produce ECM bioscaffold hydrogels.

3.3 Gelation Kinetics for ECM Bioscaffold Hydrogels

Optical density of ECM hydrogels over time revealed a logarithmic curve during the gelation period at 37°C. As expected, increased optical density of the hydrogel was observed for higher concentrations of pAdv ECM bioscaffold (Fig. 3A). Ninety percent gelation occurred within 60 minutes and peak gelation was reached within 90 minutes (Fig. 3A). A plot of the normalized absorbance of pAdv, hAdv and pSIS ECM bioscaffolds during gelation revealed similar rates of gelation among all biomaterials tested (Fig. 3B). The speed (S), t_{lag}, and $t_{1/2}$ of gelation as calculated from optical density readings of ECM hydrogel formulations were similar at the 8 mg/mL concentration for pSIS and pAdv groups (Table 2).

3.4 Mitogenic Activity of Adv Bioscaffolds is FGF2-Mediated

Primary human endothelial cells isolated from the aortic adventitia exhibited increased cell proliferation with treatment of pAdv ECM bioscaffold when compared to cells in their basal growth medium (46.1 ± 2.5 vs. 0.0 ± 7.5%, p=0.0005) (Fig. 4). Treatment of endothelial cells with pSIS ECM bioscaffolds increased cell number when compared with control cells (34.0 ± 5.8 vs. 0.0 ± 7.5%, p=0.0005). pAdv ECM bioscaffold was found to be a more potent mitogen when compared with an equivalent dose of pSIS ECM bioscaffold (46.1 ± 2.5 vs. 34.0 ± 5.8%, p=0.018). Furthermore, the effect of both ECMs was in part mediated by FGF2 since inhibition of the FGF2 signaling pathway with PD173074 prevented increases in cell number by pAdv ECM bioscaffold (25.9 ± 4.6 vs. 46.1 ± 2.5%, p=0.001) and pSIS ECM bioscaffold (18.7 ± 10.4 vs. 34.0 ± 5.8%, p=0.05). Elevated cell proliferation persisted even in the presence of FGF2 inhibitor for both pAdv ECM bioscaffold (25.9 ± 4.6 vs. 0.0 ± 7.5%, p=0.002) and pSIS ECM bioscaffold (18.7 ± 10.4 vs. 0.0 ± 7.5%, p=0.03).

3.5 Adv Bioscaffolds Promote Tube-like Structures In Vitro via FGF2

There was minimal formation of tube-like structures by human adventitia-derived endothelial cells on GFR-Matrigel substrates alone (Fig. 5A) or substrates supplemented with pepsin HCl (Fig. 5B). Addition of pAdv ECM (Fig. 5C) and pSIS ECM (Fig. 5D) bioscaffolds to GFR-Matrigel substrates enhanced formation of tube-like structures by endothelial cells when compared with cells cultured on Matrigel alone (Fig. 5A) and substrates supplemented with pepsin HCl digestion buffer alone (Fig. 5B). Addition of the FGF2 inhibitor PD173074 did not affect tube-like formation on Matrigel alone (Fig. 5E) or pepsin HCl-supplemented substrates (Fig. 5F). Conversely, PD173074 decreased the tube-like formation on pAdv ECM bioscaffold (Fig. 5G) and pSIS ECM bioscaffold-supplemented substrates (Fig. 5H) when compared with cells cultured on ECM bioscaffold-supplemented substrates in the absence of FGF2 inhibitor (Fig. 5C, D, respectively).

Quantification of the number (Fig. 5I) and total length (Fig. 5J) of tube-like structures was consistent with our qualitative observations and all values for treated cells were compared with pepsin-HCl controls. We noted minimal endothelial cell branching on Matrigel alone in the presence of DMSO or PD173074 added to the culture medium. We observed an increase in both the number and total length of tube-like structures on pAdv ECM bioscaffold containing substrates when compared with pepsin-HCl controls (151.7 ± 33.01 vs 54.7 ± 23.80 tubes, respectively, p=0.017 and 27.8 ± 4.34 vs 9.5 ± 4.15 mm, respectively, p=0.006). The presence of FGF2 inhibitor decreased the number and length of tube-like structures when compared with the absence of inhibitor for pAdv ECM bioscaffold (67.0 ± 39.89 vs 151.7 ± 33.01 tubes, p=0.049 and 10.4 ± 6.20 vs 27.8 ± 4.34 mm, p=0.020). A similar trend was noted for cells cultured on pSIS ECM-supplemented substrates when compared with pepsin-HCl controls, an observation which did not reach statistical significance (110.7 ± 36.95 vs 54.7 ± 23.80 tubes, respectively, p=0.104 and 17.9 ± 6.23 vs 9.5 ± 4.15 mm, respectively, p=0.135). The effect of FGF2 inhibition on tube-like formation on pSIS ECM-supplemented substrates was similar to that of pAdv ECM for both tube number and total tube length when compared with pepsin-HCl control but did not reach 95% confidence (44.0 ± 18.08 vs 110.7 ± 36.95 tubes, respectively, p=0.069 and 6.7 ± 2.42 vs 17.9 ± 6.23 mm, respectively, p=0.075).

3.6 In Vivo Angiogenic Activity of pAdv Bioscaffolds

To evaluate the *in vivo* angiogenic potential of pAdv ECM bioscaffold, we employed the chick CAM model for angiogenesis. Qualitative inspection of pSIS ECM bioscaffold and pAdv ECM bioscaffold-loaded fibrin scaffolds after 72 hr revealed approximately the same level of angiogenic activity evidenced by the "spoke-wheel" pattern of chick vasculature around the perimeter of the scaffolds (Fig. 6A). Digestion buffer-loaded scaffolds did not elicit any angiogenic response after 72 hr. Vascular invasion into the scaffold occurred in a dose-dependent manner with increasing pAdv ECM bioscaffold concentrations up to 250 μg/mL (Fig. 6B, arrowheads). Although 50-500 μg/mL pAdv ECM bioscaffold all resulted in a spoke-wheel pattern around the scaffold (Fig. 6A and Fig. S1), histological examination revealed abrogated a vascular invasion front at the highest dose of pAdv ECM (500 μg/mL) (Fig. 6B). Addition of the FGF2 inhibitor PD173074 completely inhibited pAdv ECM bioscaffold (250 μg/mL)-induced angiogenesis and inclusion of the drug vehicle DMSO alone had no effect on pro-angiogenic effects of pAdv ECM bioscaffold (Fig. 6C). We noted chemoattraction of lectin-negative cells invading pSIS and pAdv ECM-loaded scaffolds (Fig. 6B, asterix) ahead of a vascular front of migrating lectin-positive cells (Fig. 6B, arrowheads). Representative higher magnification images of this phenomenon for pAdv ECM-loaded scaffolds are displayed in Fig. 6D. We observed an avascular zone of lectin-negative cells within the pAdv ECM-loaded (250 μg/mL) scaffold (Fig. 6Di, asterix), preceding invasion of migrating lectin-positive cells into the scaffold (Fig. 6Di, arrowhead). At higher concentrations of pAdv ECM (500 μg/mL), lectin-negative cells invaded the scaffold whereas lectin-positive cells abutted and did not traverse the scaffold/CAM interface (Fig. 6Dii).

3.7 Detection of Angiogenesis-Related Proteins in ECM Bioscaffolds

We detected the presence of all 55 proteins on an angiogenesis-related commercial protein array in specimens of pAdv and pSIS ECM bioscaffolds as well as hAdv bioscaffolds isolated from normal and aneurysmal patients (Fig. 7). A complete list of all array proteins which were detected and densitometry values are displayed in Table 3. Qualitative inspection of array blots revealed that FGF2 was detected in all ECM bioscaffolds (Fig. 7, B19, B20). FGF1 and FGF2 (Fig. 7, B17, B18, B19, B20, respectively) were more abundant in pSIS ECM bioscaffold when compared with pAdv ECM bioscaffold (122.0 ± 4.43 vs 43.3 ± 0.7 pixel density (arbitrary units, $p=0.022$ and 100.2 ± 0.56 vs 43.5 ± 0.46 pixel density, respectively). Eight other angiogenesis-related factors were more abundant in pSIS ECM than in pAdv ECM bioscaffolds (Table 3). Interestingly, 19 proteins, including FGF2, were found to be in lower levels in hAdv ECM bioscaffold prepared from aneurysmal human aorta (>42 mm in maximal orthogonal diameter) when compared with specimens of non-aneurysmal aorta (≤34 mm) (Table 3). Of note, thrombospondin 1 (TSP1) was approximately 3 times more abundant than the average amount of all other proteins (60.0 ± 1.91 vs. 19.9 ± 1.34). None of the detected angiogenesis-related factors were found to be elevated in aneurysmal specimens when compared with normal specimens.

Discussion

Therapeutic efficacy of ECM bioscaffolds has been well demonstrated in a variety of applications where matrix preparations sourced from many tissue types are formulated into hydrogel-based biomaterials and utilized for targeted tissue-specific regeneration. [1, 46-51] In this study, we prepared a new ECM bioscaffold-based hydrogel biomaterial from a perivascular microenvironment using decellularized human and porcine aortic adventitial specimens. We characterized these ECM bioscaffolds for their matrix protein composition, microarchitecture and signaling activities on primary human endothelial cells *in vitro* and in an *in vivo* model of angiogenesis.

Using slight modifications to established techniques, [39] we demonstrated that ECM hydrogels self-assembled from pepsin-digested decellularized adventitial tissue under physiological conditions of pH, ionic strength and temperature to resemble native adventitial ECM architecture. Hydrogels derived from hAdv and pAdv ECM bioscaffolds recapitulated fibrous matrix microarchitecture in striking similarity to that of native human adventitia. These Adv ECM hydrogels exhibited a fiber morphology that appeared to be straighter and less undulated than fibers of hydrogels derived from pSIS ECM bioscaffold. The noted differences in matrix fiber ultrastructure of these hydrogels are likely dependent on the tissue-specific protein milieu which is concordantly dictated by the unique biomechanical demands of that tissue. For example, the aorta is a resilient, highly elastic tissue that endures continuous cyclic loading without overt dilatation or rupture in the absence of aneurysmal disease. Contrarily, the intestine is more porous to facilitate nutrient absorption, which may explain the observed decreased fiber density and undulated fiber morphology following ECM bioscaffold gelation. While further testing will ultimately determine the biomechanical properties of adventitia-derived ECM hydrogels, importantly, our collagen- and elastin-containing ECM bioscaffold hydrogels exhibited microarchitectural mimicry of the native adventitia following gelation.

Analysis of the gelation kinetics of Adv ECM bioscaffold hydrogels revealed a gelation rate profile similar to that of other tissue sources such as pSIS for similar concentrations. The observed similarity in gelation kinetics among pSIS and Adv ECM bioscaffold hydrogels was somewhat unexpected due to the assumed compositional differences in proteins of SIS and adventitial microenvironments. Since hydrogel formation involves interplay among self-assembling matrix proteins such as collagens and the process can be modulated by laminin, fibronectin, and proteoglycans, the interpretation of gelation activities is complex. The observed similarities between the pSIS and Adv ECM gelation kinetics suggest that unique tissues, even when processed by different decellularization procedures can be ultimately reconciled through the process of ECM bioscaffold gelation, which similarly converts these unique ECMs to a hydrogel form. ECM hydrogels across unique tissue sources could potentially be further tailored by modulating the concentration of ECM bioscaffold. We are interested in understanding the specific protein components and functionality of pAdv ECM hydrogels and the present work further focused on the inherent bioactive properties of porcine ECMs and their influence on the *in vitro* behavior of human adventitia-derived endothelial cells and on *in vivo* angiogenesis.

We evaluated the influence of endogenous FGF2 within pepsin-digested porcine ECM bioscaffolds on activities key to angiogenesis. pAdv and pSIS ECM bioscaffold-induced proliferation of endothelial cells was FGF2 mediated. The mitogenic activity of both the Adv and pSIS ECM bioscaffolds in the presence of FGF2 inhibitor remained elevated above untreated controls to indicate FGF2-independent signaling by ECM bioscaffolds that directs cell proliferation, consistent with findings in porcine urinary bladder [52] and dermis [37] ECMs. FGF2 also mediated the ECM-induced network formation of tube-like structures by human adventitia-derived endothelial cells. Importantly, pAdv ECM bioscaffolds exhibited greater mitogenic potency than pSIS ECM bioscaffold, despite the increased abundance of FGF1 and 2 in pSIS ECM bioscaffold relative to Adv ECM bioscaffold, and we make two interpretations from this observation. First, the tissue-specific milieu of the adventitia is advantageous for endothelial cells derived from this locale perhaps through retention of other tissue-specific growth factor-dependent and independent mitogenic signals. In addition or alternatively to this explanation, we l reason that bioactivity capabilities differ between pSIS and pAdv ECM bioscaffold preparations. Furthermore, we detected every protein probed by the array in all ECMs prepared in this study and the human-specific nature of the array precludes us from making direct comparisons of protein abundance in human versus porcine ECMs. Importantly, the presence of growth factors in ECM scaffolds, such as bioactive FGF2 might also contribute to maintenance of resident progenitor cell niches in the adventitia [29]. The decreased abundance of several angiogenesis-related factors in human aneurysm raises numerous questions related to disease mechanisms and offers opportunities to engineer *in vitro* models of human disease using perivascular ECM bioscaffolds and evaluate the therapeutic potential of the xenogeneic ECM counterparts *in vivo*.

Using the chick CAM *in vivo* angiogenesis model, we demonstrated the *in vivo* angiogenic potential of pAdv ECM. The vascular invasion noted with increasing concentrations of pAdv ECM bioscaffold could be attributed to the higher concentration of FGF2 and other angiogenic factors in the scaffolds. We speculate that the invasion of migrating lectin-negative cells are macrophages preceding lectin-positive endothelial cells during angiogenesis in response to pAdv and pSIS ECM-loaded scaffolds. We explain the interesting observation of inhibited vessel invasion at the highest dose of 500 μg/mL pAdv ECM bioscaffold in one of two ways. Either the present anti-angiogenic factors such as TSP1 interfere with pro-angiogenic signals or negative feedback mechanisms in the CAM are engaged by high concentrations of pro-angiogenic factors. The complete abrogation of pAdv ECM bioscaffold *in vivo* angiogenic potential in the presence of FGF2 inhibitor strongly suggests that FGF2 is a major proangiogenic signal and potent regenerative factor in adventitial ECM. Although alternative matrix signaling such as mechanotransduction and integrin-mediated signaling contribute to increased cellular proliferation, [53, 54] a review of *in vitro* angiogenic and vasculogenic models by Morin and Tranquillo affirms that the majority of the reports stated a required addition of exogenous growth factors in order to achieve angiogenesis and/or vasculogenesis with combinations of endothelial cells and pericytes when ECM bioscaffolds were not utilized. [55] Recently, the *in vivo* angiogenic potential of pSIS bioscaffold hydrogels was associated with matrix degradation-dependent release of FGF2 and VEGF. [13] Likewise, Adv ECM bioscaffold-derived hydrogels serve

as a depot for signals such as FGF2 that influence cell behaviors important for blood vessel formation.

For clinical applications, a select few ECM bioscaffold-derived hydrogels would ideally be developed to invoke regeneration in most diseased organs. Additionally, tissue-specific ECM hydrogels can serve as natural biologic scaffolds which could be useful for discovery biology of disease mechanisms. Although ECM hydrogels from a variety of tissue sources exhibited inherent bioactivity, [46-50] investigation of their impact on angiogenesis emerged only recently. [13, 25] These studies provided evidence that ECM bioscaffolds influence [56, 57] and interact with [18, 39] blood vessel cells. The angiogenic potential of hybrid scaffolds has been better studied using synthetic materials conjugated with unique combinations of tissue-derived angiogenic growth factors and must be precisely engineered for specific applications with engineered growth factor content and release profiles. [58] ECM bioscaffolds offer a distinct advantage over synthetic constructs in their tissue-specific mimicry through multi-factorial structural and signaling capacities. Furthermore, hydrogels derived from ECM bioscaffolds can be tailored for specific tissue regeneration applications through choice of source tissue, density and method of delivery. Our findings collectively demonstrate that Adv ECM bioscaffold hydrogels are versatile biological scaffolds that are capable of both microstructural and growth factor-dependent signaling mimicry of the native adventitia microenvironment which together are important for desirable effects on cellular function of blood vessel lineages.

Conclusions

We reveal that perivascular tissue from the human and porcine aortic adventitia can be decellularized to derive ECM bioscaffolds and formulated into hydrogels that recapitulate native matrix fiber microarchitecture. pAdv ECM bioscaffolds retained bioactive signals that invoked FGF2-mediated human endothelial cell proliferation, network formation of tube-like structures *in vitro*, and angiogenesis *in vivo*. Several angiogenesis-related proteins, including FGF2, are present within Adv ECM bioscaffolds and many were less abundant in matrix prepared from specimens of human aneurysm. These findings provide support for the use of Adv ECM bioscaffolds in further study of vasculogenesis and angiogenesis in normal physiology in the setting of cardiovascular disease, and also provide novel therapeutic opportunities.

Supplementary Material

Refer to Web version on PubMed Central for supplementary material.

Acknowledgements

Research reported in this publication was supported by the National Heart, Lung and Blood Institute of the National Institutes of Health under Award Numbers HL127214 (JAP), HL109132 (TGG), UPMC Health System Competitive Medical Research Fund (JAP), and the Department of Cardiothoracic Surgery. The authors gratefully acknowledge Kristin Valchar and Julie Schreiber for assistance with IRB protocols and informed patient consent and the Center for Organ Recovery and Education for assistance in obtaining donor tissues. We thank Dr. Forozan Navid for help with aortic specimen acquisition. Scanning electron microscopy was performed in the Center for Biologic Imaging (CBI), University of Pittsburgh with expert guidance from Dr. Simon Watkins, Dr. Donna Stolz and Mr. Jonathan Franks. The CBI is supported by the National Institutes of Health Award Numbers P30CA047904, P01HL114453,

P30DK072506, and P50GM082251 (SW). This project used the University of Pittsburgh Cancer Institute Cytometry Facility that is supported in part by the National Institutes of Health Award Number P30CA047904. We gratefully acknowledge the assistance of Mr. E. Michael Meyer and Dr. Vera Donnenberg in using the flow cytometry facility.

References

[1]. Wang RM, Christman KL. Decellularized myocardial matrix hydrogels: In basic research and preclinical studies. Adv Drug Deliv Rev. 2016; 96:77–82. [PubMed: 26056717]

[2]. Londono R, Badylak SF. Biologic Scaffolds for Regenerative Medicine: Mechanisms of In vivo Remodeling. Ann Biomed Eng. 2015; 43:577–92. [PubMed: 25213186]

[3]. Badylak SF, Freytes DO, Gilbert TW. Extracellular matrix as a biological scaffold material: Structure and function. Acta biomaterialia. 2009; 5:1–13. [PubMed: 18938117]

[4]. Singelyn JM, Sundaramurthy P, Johnson TD, Schup-Magoffin PJ, Hu DP, Faulk DM, et al. Catheter-deliverable hydrogel derived from decellularized ventricular extracellular matrix increases endogenous cardiomyocytes and preserves cardiac function post-myocardial infarction. J Am Coll Cardiol. 2012; 59:751–63. [PubMed: 22340268]

[5]. Wassenaar JW, Boss GR, Christman KL. Decellularized skeletal muscle as an in vitro model for studying drug-extracellular matrix interactions. Biomaterials. 2015; 64:108–14. [PubMed: 26125502]

[6]. Quint C, Arief M, Muto A, Dardik A, Niklason LE. Allogeneic human tissue-engineered blood vessel. Journal of Vascular Surgery. 2012; 55:790–8. [PubMed: 22056286]

[7]. Gubareva EA, Sjoqvist S, Gilevich IV, Sotnichenko AS, Kuevda EV, Lim ML, et al. Orthotopic transplantation of a tissue engineered diaphragm in rats. Biomaterials. 2016; 77:320–35. [PubMed: 26618750]

[8]. Fercana G, Bowser D, Portilla M, Langan EM, Carsten CG, Cull DL, et al. Platform Technologies for Decellularization, Tunic-Specific Cell Seeding, and In Vitro Conditioning of Extended Length, Small Diameter Vascular Grafts. Tissue Engineering Part C-Methods. 2014; 20:1016–27. [PubMed: 24749889]

[9]. Schulte JB, Simionescu A, Simionescu DT. The Acellular Myocardial Flap: A Novel Extracellular Matrix Scaffold Enriched with Patent Microvascular Networks and Biocompatible Cell Niches. Tissue Engineering Part C-Methods. 2013; 19:518–30. [PubMed: 23151037]

[10]. Hauschka SD, Konigsberg IR. The influence of collagen on the development of muscle clones. Proceedings of the National Academy of Sciences of the United States of America. 1966; 55:119–26. [PubMed: 5220860]

[11]. Keane TJ, Dziki J, Sobieski E, Smoulder A, Castleton A, Turner N, et al. Restoring Mucosal Barrier Function and Modifying Macrophage Phenotype with an Extracellular Matrix Hydrogel: Potential Therapy for Ulcerative Colitis. Journal of Crohn's & colitis. 2016

[12]. Huleihel L, Hussey GS, Naranjo JD, Zhang L, Dziki JL, Turner NJ, et al. Matrix-bound nanovesicles within ECM bioscaffolds. Science advances. 2016; 2:e1600502. [PubMed: 27386584]

[13]. Wang W, Zhang X, Chao NN, Qin TW, Ding W, Zhang Y, et al. Preparation and characterization of pro-angiogenic gel derived from small intestinal submucosa. Acta Biomaterialia. 2016; 29:135–48. [PubMed: 26472613]

[14]. Seif-Naraghi SB, Horn D, Schup-Magoffin PJ, Christman KL. Injectable extracellular matrix derived hydrogel provides a platform for enhanced retention and delivery of a heparin-binding growth factor. Acta Biomater. 2012; 8:3695–703. [PubMed: 22750737]

[15]. McDevitt CA, Wildey GM, Cutrone RM. Transforming growth factor-beta1 in a sterilized tissue derived from the pig small intestine submucosa. J Biomed Mater Res A. 2003; 67:637–40. [PubMed: 14566807]

[16]. Hodde JP, Record RD, Liang HA, Badylak SF. Vascular endothelial growth factor in porcine-derived extracellular matrix. Endothelium. 2001; 8:11–24. [PubMed: 11409848]

[17]. Voytik-Harbin SL, Brightman AO, Kraine MR, Waisner B, Badylak SF. Identification of extractable growth factors from small intestinal submucosa. J Cell Biochem. 1997; 67:478–91. [PubMed: 9383707]

[18]. Sicari BM, Rubin JP, Dearth CL, Wolf MT, Ambrosio F, Boninger M, et al. An Acellular Biologic Scaffold Promotes Skeletal Muscle Formation in Mice and Humans with Volumetric Muscle Loss. Science Translational Medicine. 2014; 6

[19]. Hoshiba T, Chen GP, Endo C, Maruyama H, Wakui M, Nemoto E, et al. Decellularized Extracellular Matrix as an In Vitro Model to Study the Comprehensive Roles of the ECM in Stem Cell Differentiation. Stem Cells International. 2016

[20]. Cortiella J, Niles J, Cantu A, Brettler A, Pham A, Vargas G, et al. Influence of Acellular Natural Lung Matrix on Murine Embryonic Stem Cell Differentiation and Tissue Formation. Tissue Engineering Part A. 2010; 16:2565–80. [PubMed: 20408765]

[21]. Leiros GJ, Kusinsky AG, Drago H, Bossi S, Sturla F, Castellanos ML, et al. Dermal Papilla Cells Improve the Wound Healing Process and Generate Hair Bud-Like Structures in Grafted Skin Substitutes Using Hair Follicle Stem Cells. Stem Cells Translational Medicine. 2014; 3:1209–19. [PubMed: 25161315]

[22]. Bonandrini B, Figliuzzi M, Papadimou E, Morigi M, Perico N, Casiraghi F, et al. Recellularization of Well-Preserved Acellular Kidney Scaffold Using Embryonic Stem Cells. Tissue Engineering Part A. 2014; 20:1486–98. [PubMed: 24320825]

[23]. Constantinescu A, Andrei E, Iordache F, Constantinescu E, Maniu H. Recellularization potential assessment of Wharton's Jelly-derived endothelial progenitor cells using a human fetal vascular tissue model. In Vitro Cellular & Developmental Biology-Animal. 2014; 50:937–44. [PubMed: 25124869]

[24]. Discher DE, Mooney DJ, Zandstra PW. Growth Factors, Matrices, and Forces Combine and Control Stem Cells. Science. 2009; 324:1673–7. [PubMed: 19556500]

[25]. Liu SY, Zhang HM, Zhang XJ, Lu W, Huang XH, Xie H, et al. Synergistic Angiogenesis Promoting Effects of Extracellular Matrix Scaffolds and Adipose-Derived Stem Cells During Wound Repair. Tissue Engineering Part A. 2011; 17:725–39. [PubMed: 20929282]

[26]. Flaumenhaft R, Rifkin DB. The Extracellular Regulation of Growth-Factor Action. Molecular Biology of the Cell. 1992; 3:1057–65. [PubMed: 1421565]

[27]. Rifkin DB. Cross-talk among proteases and matrix in the control of growth factor action. Fibrinolysis & Proteolysis. 1997; 11:3–9.

[28]. Stenmark KR, Yeager ME, El Kasmi KC, Nozik-Grayck E, Gerasimovskaya EV, Li M, et al. The Adventitia: Essential Regulator of Vascular Wall Structure and Function. Annual Review of Physiology. 2013; 75:23–47. 75.

[29]. Majesky MW, Dong XR, Hoglund V, Daum G, Mahoney WM Jr. The adventitia: a progenitor cell niche for the vessel wall. Cells Tissues Organs. 2012; 195:73–81. [PubMed: 22005572]

[30]. Majesky MW. Adventitia and perivascular cells. Arterioscler Thromb Vasc Biol. 2015; 35:e31–5. [PubMed: 26203160]

[31]. Hodde JP, Badylak SF, Brightman AO, Voytik-Harbin SL. Glycosaminoglycan content of small intestinal submucosa: a bioscaffold for tissue replacement. Tissue Eng. 1996; 2:209–17. [PubMed: 19877943]

[32]. Okada M, Payne TR, Oshima H, Momoi N, Tobita K, Huard J. Differential efficacy of gels derived from small intestinal submucosa as an injectable biomaterial for myocardial infarct repair. Biomaterials. 2010; 31:7678–83. [PubMed: 20674011]

[33]. Shi L, Ronfard V. Biochemical and biomechanical characterization of porcine small intestinal submucosa (SIS): a mini review. Int J Burns Trauma. 2013; 3:173–9. [PubMed: 24273692]

[34]. Valentin JE, Stewart-Akers AM, Gilbert TW, Badylak SF. Macrophage participation in the degradation and remodeling of extracellular matrix scaffolds. Tissue Eng Part A. 2009; 15:1687–94. [PubMed: 19125644]

[35]. Badylak SF, Lantz GC, Coffey A, Geddes LA. Small Intestinal Submucosa as a Large Diameter Vascular Graft in the Dog. Journal of Surgical Research. 1989; 47:74–80. [PubMed: 2739401]

[36]. Lantz GC, Badylak SF, Coffey AC, Geddes LA, Blevins WE. Small intestinal submucosa as a small-diameter arterial graft in the dog. Journal of investigative surgery : the official journal of the Academy of Surgical Research. 1990; 3:217–27. [PubMed: 2078544]

[37]. Reing JE, Brown BN, Daly KA, Freund JM, Gilbert TW, Hsiong SX, et al. The effects of processing methods upon mechanical and biologic properties of porcine dermal extracellular matrix scaffolds. Biomaterials. 2010; 31:8626–33. [PubMed: 20728934]

[38]. Phillippi JA, Green BR, Eskay MA, Kotlarczyk MP, Hill MR, Robertson AM, et al. Mechanism of aortic medial matrix remodeling is distinct in patients with bicuspid aortic valve. J Thorac Cardiovasc Surg. 2014; 147:1056–64. [PubMed: 23764410]

[39]. Freytes DO, Martin J, Velankar SS, Lee AS, Badylak SF. Preparation and rheological characterization of a gel form of the porcine urinary bladder matrix. Biomaterials. 2008; 29:1630–7. [PubMed: 18201760]

[40]. Zimmerlin L, Donnenberg VS, Pfeifer ME, Meyer EM, Peault B, Rubin JP, et al. Stromal vascular progenitors in adult human adipose tissue. Cytometry A. 2010; 77:22–30. [PubMed: 19852056]

[41]. Smith JD, Fisher GW, Waggoner AS, Campbell PG. The use of quantum dots for analysis of chick CAM vasculature. Microvasc Res. 2007; 73:75–83. [PubMed: 17070560]

[42]. Smith JD, Melhem ME, Magge KT, Waggoner AS, Campbell PG. Improved growth factor directed vascularization into fibrin constructs through inclusion of additional extracellular molecules. Microvasc Res. 2007; 73:84–94. [PubMed: 17223139]

[43]. Smith JD, Melhem ME, Magge KT, Waggoner AS, Campbell PG. Improved growth factor directed vascularization into fibrin constructs through inclusion of additional extracellular molecules. Microvasc Res. 2007; 73:84–94. [PubMed: 17223139]

[44]. Smith JD, Fisher GW, Waggoner AS, Campbell PG. The use of quantum dots for analysis of chick CAM vasculature. Microvasc Res. 2007; 73:75–83. [PubMed: 17070560]

[45]. Jadlowiec J, Dongell D, Smith J, Conover C, Campbell P. Pregnancy-associated plasma protein-a is involved in matrix mineralization of human adult mesenchymal stem cells and angiogenesis in the chick chorioallontoic membrane. Endocrinology. 2005; 146:3765–72. [PubMed: 15919757]

[46]. Hong Y, Huber A, Takanari K, Amoroso NJ, Hashizume R, Badylak SF, et al. Mechanical properties and in vivo behavior of a biodegradable synthetic polymer microfiber-extracellular matrix hydrogel biohybrid scaffold. Biomaterials. 2011; 32:3387–94. [PubMed: 21303718]

[47]. Wolf MT, Daly KA, Brennan-Pierce EP, Johnson SA, Carruthers CA, D'Amore A, et al. A hydrogel derived from decellularized dermal extracellular matrix. Biomaterials. 2012; 33:7028–38. [PubMed: 22789723]

[48]. Zhang L, Zhang F, Weng ZF, Brown BN, Yan HQ, Ma XM, et al. Effect of an Inductive Hydrogel Composed of Urinary Bladder Matrix Upon Functional Recovery Following Traumatic Brain Injury. Tissue Engineering Part A. 2013; 19:1909–18. [PubMed: 23596981]

[49]. Medberry CJ, Crapo PM, Siu BF, Carruthers CA, Wolf MT, Nagarkar SP, et al. Hydrogels derived from central nervous system extracellular matrix. Biomaterials. 2013; 34:1033–40. [PubMed: 23158935]

[50]. Sawkins MJ, Bowen W, Dhadda P, Markides H, Sidney LE, Taylor AJ, et al. Hydrogels derived from demineralized and decellularized bone extracellular matrix. Acta Biomaterialia. 2013; 9:7865–73. [PubMed: 23624219]

[51]. Dahl SL, Koh J, Prabhakar V, Niklason LE. Decellularized native and engineered arterial scaffolds for transplantation. Cell Transplant. 2003; 12:659–66. [PubMed: 14579934]

[52]. Reing JE, Zhang L, Myers-Irvin J, Cordero KE, Freytes DO, Heber-Katz E, et al. Degradation products of extracellular matrix affect cell migration and proliferation. Tissue Eng Part A. 2009; 15:605–14. [PubMed: 18652541]

[53]. Ruoslahti E. RGD and other recognition sequences for integrins. Annu Rev Cell Dev Biol. 1996; 12:697–715. [PubMed: 8970741]

[54]. Bissell MJ, Barcellos-Hoff MH. The influence of extracellular matrix on gene expression: is structure the message? J Cell Sci Suppl. 1987; 8:327–43. [PubMed: 3332665]

[55]. Morin KT, Tranquillo RT. In vitro models of angiogenesis and vasculogenesis in fibrin gel. Experimental Cell Research. 2013; 319:2409–17. [PubMed: 23800466]

[56]. Agrawal V, Tottey S, Johnson SA, Freund JM, Siu BF, Badylak SF. Recruitment of progenitor cells by an extracellular matrix cryptic peptide in a mouse model of digit amputation. Tissue Eng Part A. 2011; 17:2435–43. [PubMed: 21563860]

[57]. Maquart FX, Bellon G, Pasco S, Monboisse JC. Matrikines in the regulation of extracellular matrix degradation. Biochimie. 2005; 87:353–60. [PubMed: 15781322]

[58]. Rufaihah AJ, Seliktar D. Hydrogels for therapeutic cardiovascular angiogenesis. Adv Drug Deliv Rev. 2016; 96:31–9. [PubMed: 26212158]

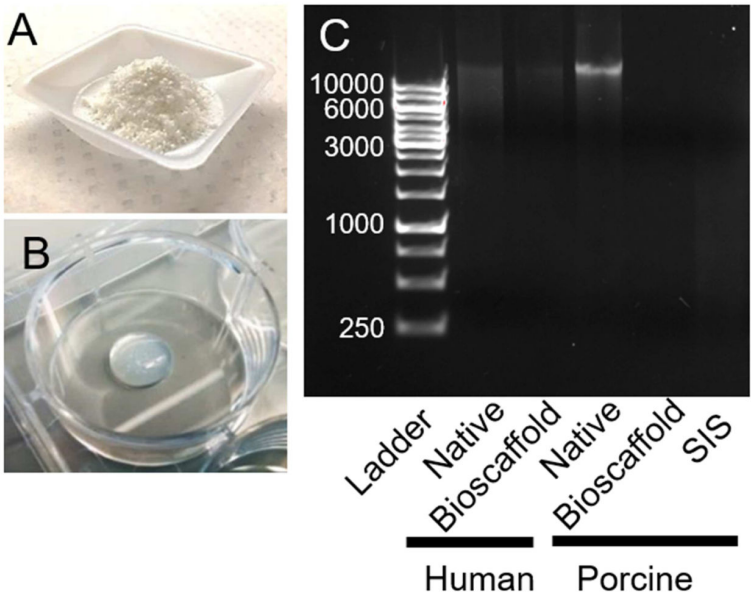

Figure 1.

Preparation and characterization of ECM bioscaffolds. A) ECM bioscaffold as a lyophilized ground powder. B) Hydrogel formation from pH-neutralized pepsin-digested ECM bioscaffolds after 1 hr at 37°C. C) DNA extracts from 1.2 mg total tissue weight were qualitatively analyzed using ethidium bromide-containing agarose gel electrophoresis.

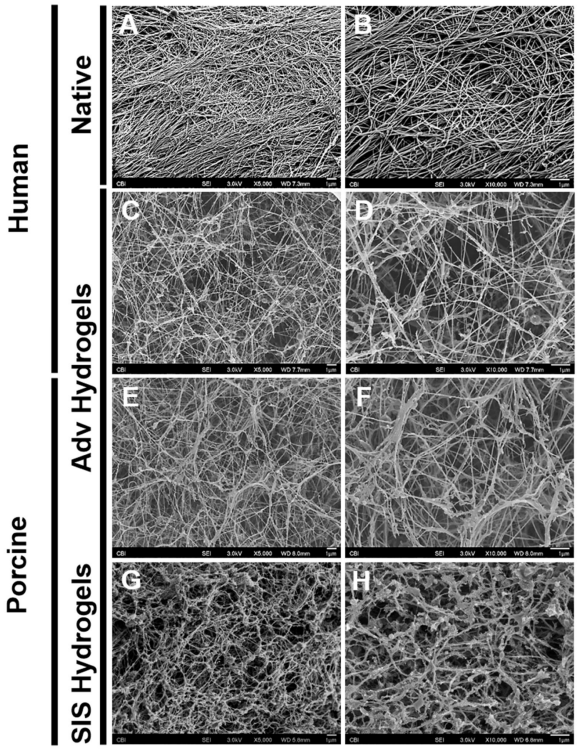

Figure 2.

Scanning electron microscopy of adventitial ECM hydrogel. Decellularized tissue and ECM hydrogels were fixed in 2.5% glutaraldehyde and processed for scanning electron microscopy. Representative micrographs showing decellularized human adventitia (Adv) (A-B), human Adv hydrogel (C-D), porcine Adv hydrogel (E-F) and porcine small intestinal submucosa (SIS) hydrogel (G-H) at 5,000X (A, C, E) and 10,000X (B, D, F) magnifications. All scale bars=1μm.

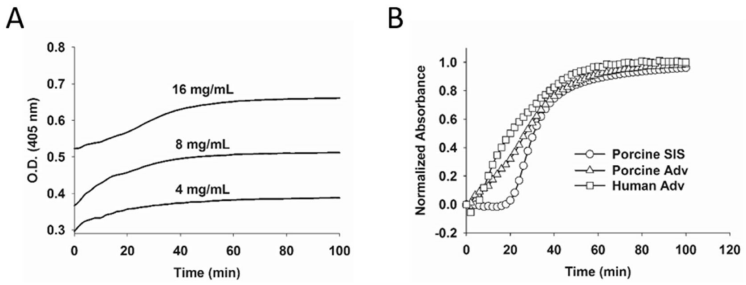

Figure 3.

Turbidimetric gelation kinetics of ECM hydrogels. Gelation of pH-neutralized ECM digests was monitored using optical density (O.D.) readings at 405 nm at 37°C for 90 min. A) Porcine adventitia (Adv) (4, 8 and 16 mg/mL). B) Normalized turbidimetric gelation kinetics of porcine SIS (8 mg/mL), human Adv and porcine Adv (16 mg/mL).

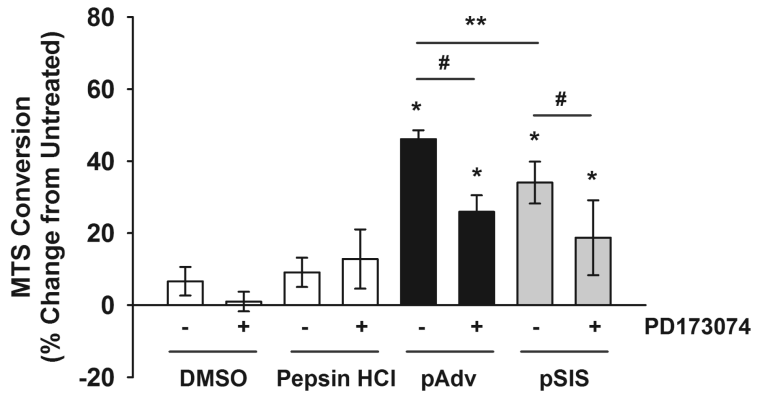

Figure 4.

FGF2-mediated stimulation of primary endothelial cell proliferation by ECMs. Primary human adventitia-derived endothelial cells were cultured in the presence of 10 μg/mL porcine adventitial (pAdv, solid bars) or porcine small intestinal submucosa (pSIS, gray bars) ECM. Cells in their basal culture medium, FGF2 inhibitor alone (100 nM PD173074 in DMSO), or an equivalent volume of DMSO and digestion buffer (1 mg/mL pepsin in 0.01 N HCl) served as controls (open bars). Quantification of MTS conversion was performed after 72 hr of exposure to the above conditions using a commercial assay and results were expressed as percent change of untreated cells. One representative of three independent experiments is displayed. Bars represent mean of four assay replicates ± standard deviation. * indicates $p<0.05$ when compared with untreated condition, **indicates $p<0.02$, and # indicates $p<0.005$.

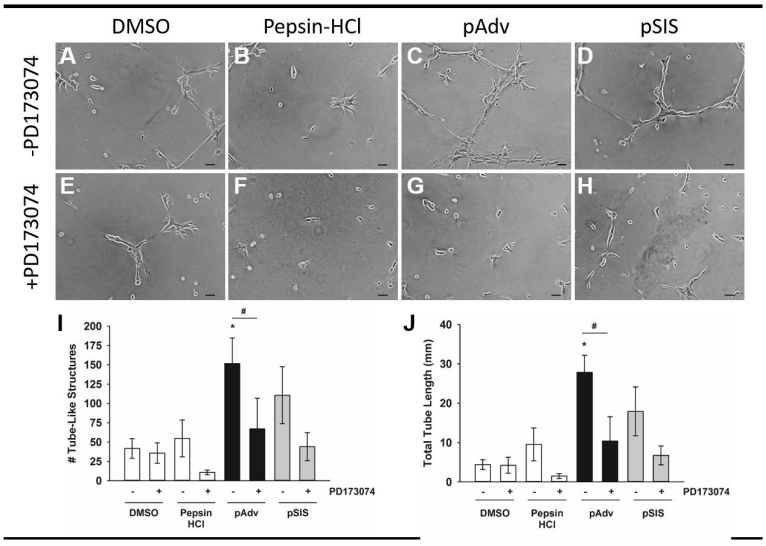

Figure 5.

Effect of ECM bioscaffolds on network formation of tube-like structures *in vitro*. Human adventitia-derived endothelial cells were cultured on growth factor reduced-Matrigel substrates: A) DMSO, 0.05% (v/v), B) Digestion buffer (1% (w/v) Pepsin in 0.1 N HCl), C) pAdv ECM, and D) pSIS ECM. FGF2 inhibitor PD173074 (100 nM) was added to the culture medium of above treatments shown in parallel wells (E-H). A-H: One representative 10X field is shown, selected from one of three replicates of two independent experiments. All scale bars= 50 μm for A-H. Quantification of the number (I) and total length (J) of tube-like structures from 5×5 stitched fields captured at 10X for non-ECM-supplemented (open bars), pAdv (solid bars) and pSIS (gray bars) ECM-supplemented substrates in the absence and presence of PD173074. Bars represent mean of three assay replicates ± standard deviation. Images and graphs represent data from one of two independent experiments. *Significant from pepsin HCl, $p<0.02$; #Significant from pAdv ECM-treated cells in the absence of PD173074, $p<0.03$.

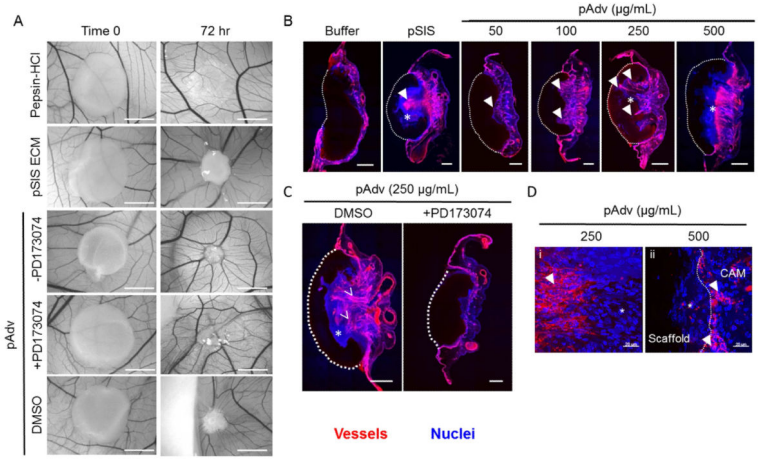

Figure 6.

Effect of ECM bioscaffolds on angiogenesis *in vivo*. A) Representative bright field images of scaffolds before (Time 0) and after (72 hr) incubation on the chorioallantoic membrane (CAM) of the chick embryo. The pro-angiogenic response to pSIS and pAdv ECM-containing fibrin scaffolds (250 μg/mL) is revealed by the spoke-wheel pattern along the perimeter of the scaffolds. There was no appreciable angiogenic response detected around scaffolds loaded with digestion buffer (1% (w/v) pepsin in 0.1 N HCl) or DMSO. Addition of the FGF2 inhibitor PD173074 (100 nM) abrogated the angiogenic response to pAdv ECM. Addition of the inhibitor vehicle only (DMSO) did not alter the angiogenic response to pAdv ECM. All scale bars for panel A = 5mm. B) Representative histological cross-sections of CAM assay scaffolds. The CAM vasculature was visualized using injected tomato lectin-Dylight® 650 (red) and nuclei are labeled with Hoechst dye (blue). A dashed white line denotes the scaffold/CAM interface. Scaffolds loaded with digestion buffer alone exhibited no vessel invasion. pSIS ECM (250 μg/mL) stimulated invasion of new vasculature (denoted by arrowheads) toward the scaffold as did pAdv ECM in a dose-dependent manner for concentrations 50-250 μg/mL. The maximum tested dose of pAdv ECM (500 μg/mL) inhibited invasion of blood vessels into the scaffold. C) Addition of DMSO did not alter pAdv ECM-induced invasion of blood vessels and FGF2 inhibitor PD173074 blocked the effect of pAdv ECM-loaded scaffolds. All scale bars in panels B and C= 500 μm. *Avascular zone comprised of lectin-negative cells. D). Representative histological cross-sections showing chemoattraction of lectin-negative cells in an avascular zone (*) adjacent to invading lectin-positive cells (arrowheads) in pAdv ECM-loaded fibrin scaffold (250 μg/mL) (i) and inhibition of invasion of lectin-positive cells in 500 μg/ml pAdv ECM-loaded fibrin scaffold (ii). (*) avascular zone comprised of lectin-negative cells, (arrowheads) vascular zone of lectin-positive cells. All scale bars for panel D = 20 μm.

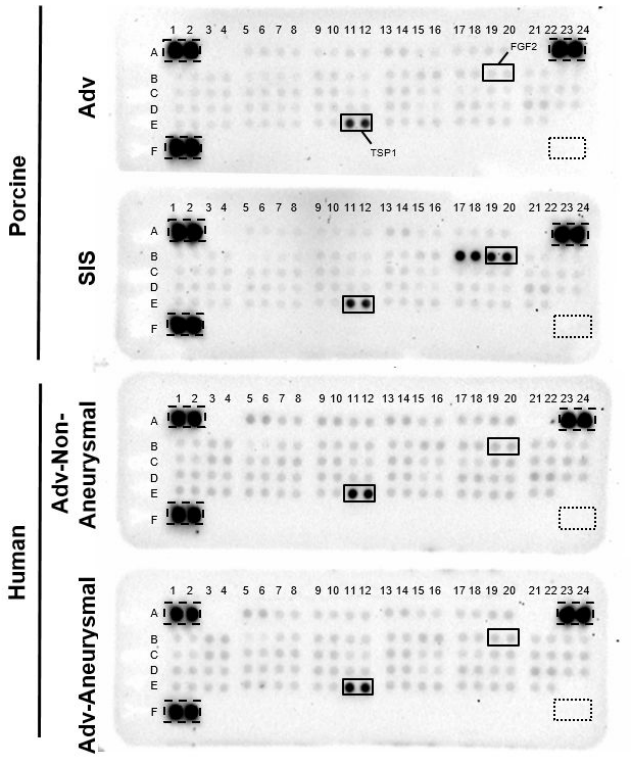

Figure 7.

Protein array-based profile of angiogenesis-related proteins. Lyophilized ECM bioscaffolds (300 μg total protein) were evaluated for the presence of 55 angiogenesis-related proteins in duplicate using the Human Angiogenesis Proteome Profiler Array. Densitometric values are provided in Table 3. Images for porcine and human ECM blots reflect exposure times of 20 min and 10 min respectively. Dashed line boxes=positive control reference spots. Dotted line boxes=negative control reference spots.

Table 1

Pepsin-soluble collagen and α-elastin content in native adventitia and adventitia-derived ECM digest from porcine and human aorta. Data are shown as mean (standard deviation).

Species	Specimen	Collagen (μg/mg tissue)	Elastin (μg/mg tissue)
Porcine	Native	2.75 (0.54)	3.61 (0.96)
	ECM Bioscaffold	18.0 (3.10)	1.95 (0.21)
Human	Native	0.56 (0.08)	1.35 (0.04)
	ECM Bioscaffold	21.2 (0.56)	3.71 (0.66)

Table 2

Turbidimetric analysis of porcine bioscaffold gelation kinetics. Representative calculations from one of three independent batches of pepsin-digested bioscaffolds are displayed. Data are shown as mean (standard deviation). S, $t_{1/2}$, and t_{lag} indicate gelation speed, time required for 50% gelation, and lag phase respectively. O.D. = optical density.

Material	Density (mg/mL)	S (OD/min)	$t_{1/2}$ (min)	t_{lag} (min)
SIS	8	0.04 (0.002)	29.3 (2.31)	17.59 (2.17)
Adventitia	4	0.02 (0.001)	30.7 (1.15)	1.96 (1.26)
	8	0.03 (0.005)	32.0 (3.46)	9.76 (8.09)
	16	0.03 (0.002)	34.0 (2.00)	14.16 (3.73)

Table 3

Angiogenesis-related protein array. Decellularized adventitia from normal (n=7 patients pooled) and aneurysmal (n=28 pooled patients) human aorta, porcine adventitia and SIS were analyzed for 55 angiogenesis-related proteins. Values represent mean pixel density of two assay replicates ± standard deviation (S.D.) for chemiluminescence detected after 5 (human ECMs) or 14 (porcine ECMs) minutes of exposure.

			Porcine		Human	
Array Key	**Protein**	**Gene ID**	**Adventitia Mean (S.D.)**	**SIS Mean (S.D.)**	**Adventitia-Normal Aorta Mean (S.D.)**	**Adventitia - Aneurysmal Aorta Mean (S.D.)**
A1, A2	Reference spots	N/A	-	-	-	-
A5, A6	Activin A	3624	44.9 (0.27)	44.5 (0.08)	25.6 (0.52)	22.2 (0.14)
A7, A8	ADAMTS-1	9510	43.7 (0.56)	47.2 (2.41)	20.6 (0.09)	18.4 (0.33)#
A9, A10	Angiogenin	283	42.5 (0.09)	51.4 (1.27)	23.3 (0.07)	18.5 (0.30)#
A11, A12	Angiopoietin-1	284	43.6 (0.41)	47.3 (1.51)	21.2 (0.06)	18.7 (0.30)
A13, A14	Angiopoietin-2	258	45.5 (0.17)	47.8 (0.03)*	23.2 (0.05)	20.1 (0.24)#
A15, A16	Angiostatin/Plasminogen	5340	42.9 (0.22)	43.5 (0.61)	19.8 (0.00)	17.7 (0.32)
A17, A18	Amphiregulin	374	43.8 (0.32)	43.7 (0.20)	20.7 (0.09)	18.0 (0.15)#
A19, A20	Artemin	9048	44.7 (0.08)	43.6 (0.34)	22.6 (0.35)	19.9 (0.05)#
A23, A24	Reference spots	N/A	-	-	-	-
B1, B2	Coagulation factor III	2152	44.3 (0.44)	44.0 (0.71)	20.2 (0.60)	18.7 (0.09)
B3, B4	CXCL16	58191	42.5 (0.24)	43.6 (0.36)	21.2 (0.49)	21.4 (0.30)
B5, B6	DPPIV	1803	44.0 (0.05)	41.3 (0.51)	17.2 (0.05)	16.7 (0.13)
B7, B8	EGF	1950	44.7 (0.08)	44.9 (1.88)	19.2 (0.23)	18.3 (0.22)#
B9, B10	EG-VEGF	84432	46.3 (0.03)	50.8 (1.58)	20.2 (0.15)	19.5 (0.20)
B11, B12	Endoglin	2022	44.0 (0.27)	45.4 (1.47)	20.6 (0.17)	18.6 (0.20)#
B13, B14	Endostatin/Col 18	80781	42.2 (0.11)	43.9 (0.09)*	20.0 (0.31)	19.7 (0.04)
B15, B16	Endothelin-1	1906	44.9 (0.40)	45.6 (0.67)	22.2 (0.48)	21.5 (0.22)
B17, B18	FGF-acidic	2246	43.3 (0.70)	122.0 (4.43)*	21.7 (0.05)	19.5 (0.18)#

			Porcine		Human	
Array Key	**Protein**	**Gene ID**	**Adventitia Mean (S.D.)**	**SIS Mean (S.D.)**	**Adventitia-Normal Aorta Mean (S.D.)**	**Adventitia - Aneurysmal Aorta Mean (S.D.)**
B19, B20	FGF-basic	2263	43.5 (0.46)	100.2 (0.56) *	22.9 (0.00)	20.6 (0.01) #
B21, B22	FGF4	2249	44.6 (0.18)	43.4 (0.74)	20.3 (0.26)	18.2 (0.37) #
B23, B24	FGF7	2252	43.9 (0.38)	45.0 (0.70)	19.8 (0.22)	19.7 (0.00)
C1, C2	GDNF	2668	43.7 (0.74)	44.7 (0.79)	20.0 (0.13)	18.0 (0.58)
C3, C4	GM-CSF	1437	44.4 (0.16)	43.9 (0.31)	22.9 (0.34)	22.2 (0.49)
C5. C6	HB-EGF	1839	45.1 (0.16)	43.7 (0.06) *	20.4 (0.19)	19.7 (0.19)
C7, C8	HGF	3082	44.6 (0.84)	46.0 (1.17)	22.1 (0.03)	20.6 (0.51)
C9, C10	IGFBP-1	3484	44.9 (0.10)	50.1 (0.53) *	22.0 (0.04)	21.1 (0.06) #
C11, C12	IGFBP-2	3485	42.2 (0.25)	44.6 (1.19)	19.5 (0.10)	18.3 (0.05) #
C13, C14	IGFBP-3	3486	45.5 (0.37)	45.7 (0.16)	22.1 (0.22)	21.3 (0.13)
C15, C16	IL1-β	3553	42.8 (0.22)	43.1 (0.16)	19.2 (0.21)	18.7 (0.23)
C17, C18	IL-8	3576	42.0 (0.05)	45.7 (0.50)	19.4 (0.02)	18.5 (0.17)
C19, C20	LAP (TGF-β1)	7040	41.5 (1.52)	46.0 (0.61)	22.1 (0.08)	20.0 (0.19) #
C21, C22	Leptin	3952	43.3 (0.09)	43.6 (0.91)	21.8 (0.12)	19.8 (0.04) #
C23, C24	MCP-1	6347	43.1 (0.79)	44.6 (0.28)	23.2 (0.22)	20.8 (0.61)
D1, D2	MIP-1α	6348	43.8 (0.13)	44.8 (0.52)	22.4 (0.12)	20.9 (0.01) #
D3, D4	MMP-8	4317	43.6 (0.31)	43.3 (0.15)	21.1 (0.85)	20.8 (0.47)
D5, D6	MMP-9	4218	44.9 (0.04)	44.4 (0.39)	21.1 (0.09)	21.0 (0.02)
D7, D8	NRG1-β1	3084	43.2 (0.28)	44.3 (1.45)	20.9 (0.02)	20.3 (0.33)
D9, D10	Pentraxin 3	5806	44.5 (0.36)	48.8 (0.07) *	21.7 (0.16)	21.3 (0.18)
D11, D12	PD-ECGF	1890	46.3 (0.23)	46.8 (1.67)	21.7 (0.51)	21.3 (0.38)
D13, D14	PDGF-AA	5154	44.7 (0.12)	44.4 (0.05)	21.6 (0.04)	21.0 (0.15)

			Porcine		Human	
Array Key	**Protein**	**Gene ID**	**Adventitia Mean (S.D.)**	**SIS Mean (S.D.)**	**Adventitia-Normal Aorta Mean (S.D.)**	**Adventitia - Aneurysmal Aorta Mean (S.D.)**
D15, D16	PDGF-BB	5155	41.6 (0.19)	42.3 (0.32)	18.5 (0.41)	18.5 (0.26)
D17, D18	Persephin	5623	45.0 (0.11)	44.7 (0.63)	22.9 (0.24)	21.4 (0.10)#
D19, D20	Platelet factor 4	5196	41.8 (0.66)	43.2 (0.07)	21.9 (0.13)	19.5 (0.43)
D21, D22	PlGF	5228	47.0 (0.47)	48.5 (0.25)	25.5 (0.32)	22.9 (0.14)#
D23, D24	Prolactin	5617	42.6 (0.34)	44.2 (0.81)*	21.6 (0.50)	19.5 (0.16)
E1, E2	Serpin B5	5268	41.8 (0.51)	48.4 (0.44)*	23.2 (0.25)	21.5 (0.17)#
E3, E4	Serpin E1	5054	42.4 (0.69)	43.2 (0.47)	22.5 (0.46)	20.6 (0.49)
E5, E6	Serpin F1	5176	43.2 (0.21)	44.0 (0.18)	21.6 (0.15)	22.2 (1.00)
E7, E8	TIMP-1	7076	43.7 (0.19)	44.6 (1.09)	20.3 (0.25)	19.5 (0.18)
E9, E10	TIMP-4	7079	43.8 (0.68)	47.5 (0.42)*	21.0 (0.32)	19.9 (0.52)
E11, E12	Thrombospondin-1	7057	86.2 (0.22)	88.9 (3.50)	63.3 (1.42)	60.0 (1.91)
E13, E14	Thrombospondin-2	7058	43.5 (1.09)	44.0 (0.08)	21.1 (0.05)	20.8 (0.07)
E15, E16	uPA	5328	43.1 (0.77)	45.2 (0.15)	20.5 (0.45)	20.5 (0.32)
E17, E18	Vasohibin	22846	44.7 (0.27)	44.1 (0.30)	21.2 (0.39)	20.3 (0.16)
E19, E20	VEGF	7422	44.1 (0.44)	44.2 (0.38)	22.0 (0.29)	19.9 (0.33)#
E21, E22	VEGF-C	7424	45.5 (0.03)	44.4 (0.49)	21.0 (0.00)	18.7 (0.31)
F1, F2	Reference spots	N/A	-	-	-	-
F23, F24	Negative control spots	N/A	-	-	-	-

* $p<0.05$ when compared with porcine adventitia;

# $p<0.05$ when compared with normal human aortic adventitial specimens.